coatings

MDPI

Article

Electrophoretic Deposition and Characterization of Chitosan/Eudragit E 100 Coatings on Titanium Substrate

Łukasz Pawłowski [1,*], Michał Bartmański [1], Gabriel Strugała [1], Aleksandra Mielewczyk-Gryń [2], Magdalena Jażdżewska [1] and Andrzej Zieliński [1]

[1] Faculty of Mechanical Engineering, Gdańsk University of Technology, Narutowicza 11/12, 80-233 Gdańsk, Poland; michal.bartmanski@pg.edu.pl (M.B.); gabriel.strugala@pg.edu.pl (G.S.); magdalena.jazdzewska@pg.edu.pl (M.J.); andrzej.zielinski@pg.edu.pl (A.Z.)

[2] Faculty of Applied Physics and Mathematics, Gdańsk University of Technology, Narutowicza 11/12, 80-233 Gdańsk, Poland; alegryn@pg.edu.pl

* Correspondence: lukasz.pawlowski@pg.edu.pl; Tel.: +48-883-797-081

Received: 29 May 2020; Accepted: 26 June 2020; Published: 28 June 2020

Abstract: Currently, a significant problem is the production of coatings for titanium implants, which will be characterized by mechanical properties comparable to those of a human bone, high corrosion resistance, and low degradation rate in the body fluids. This paper aims to describe the properties of novel chitosan/Eudragit E 100 (chit/EE100) coatings deposited on titanium grade 2 substrate by the electrophoretic technique (EPD). The deposition was carried out for different parameters like the content of EE100, time of deposition, and applied voltage. The microstructure, surface roughness, chemical and phase composition, wettability, mechanical and electrochemical properties, and degradation rate at different pH were examined in comparison to chitosan coating without the addition of Eudragit E 100. The applied deposition parameters significantly influenced the morphology of the coatings. The chit/EE100 coating with the highest homogeneity was obtained for Eudragit content of 0.25 g, at 10 V, and for 1 min. Young's modulus of this sample (24.77 ± 5.50 GPa) was most comparable to that of human cortical bone. The introduction of Eudragit E 100 into chitosan coatings significantly reduced their degradation rate in artificial saliva at neutral pH while maintaining high sensitivity to pH changes. The chit/EE100 coatings showed a slightly lower corrosion resistance compared to the chitosan coating, however, significantly exceeding the substrate corrosion resistance. All prepared coatings were characterized by hydrophilicity.

Keywords: titanium; chitosan; Eudragit; electrophoretic deposition; nanoindentation; pH-sensitive coatings; wettability

1. Introduction

Titanium and titanium alloys are materials often used in biomedical applications due to their high biocompatibility, high corrosion resistance, and low Young's modulus comparing to other metallic biomaterials. These properties promote their use as orthopedic and dental implants, orthodontic wires and brackets, and other biomedical devices [1–3]. Titanium and its alloys are often subjected to improving their osseointegration properties, resistance to corrosion, and protection against the development of bacterial infections by modification of the surface topography and the deposition of bioactive materials, e.g., calcium phosphates and bioglasses [4–7].

Currently, so-called smart polymers that respond to the external environment are gathering considerable interest. These materials change their properties under the influence of temperature, pH, UV–Vis radiation, electric, and magnetic field effects [8–12]. Among the most popular polymers are chitosan [13] and Eudragit E 100 (EE100)–methacrylic acid copolymer [14].

Chitosan, due to its biodegradability, biocompatibility, nontoxicity, and antibacterial activity, is often used in controlled drug delivery systems, wound healing, and tissue regeneration [15,16]. It is commonly applied in different forms, such as membranes, nanogels, micro/nanoparticles, films, and hydrogels [17–19]. Chitosan coatings are gathering more interest in implantology, however, they show low mechanical properties and low stability at neutral pH [20,21]. Chitosan rapidly absorbs water and is characterized by a high swelling degree in aqueous environments, leading to fast drug release [22]. Hence, co-deposition of chitosan with other biopolymers (e.g., gelatin) or nanomaterials (e.g., silver nanoparticles, gold nanoparticles, carbon nanotubes) is performed to overcome these problems [23–25]. One of the modifiers of chitosan coatings may be EE100.

Eudragits are a group of biopolymer materials that have been used in controlled drug delivery systems for several years. Depending on their functional groups, they are usually divided into polycations and polyanions [26]. Polycations include Eudragits E with dimethylamino groups, and RL, ES, NE with quaternary amino groups, while polyanions include Eudragits L and S with carboxyl groups [27]. Eudragit E 100 copolymer is based on dimethylaminoethyl methacrylate, butyl methacrylate, and methyl methacrylate with a ratio of 2:1:1 and belongs to the group of cationic polymers. It is sensitive to pH changes, dissolves in acidic environments due to amino groups, but is insoluble at neutral pH [28]. In an alkaline environment, the polymer swells [29]. It is most often used for coatings on pills to transport the drug substance to the appropriate part of the digestive tract, mainly the stomach, because of its good adhesion, low viscosity, and good ability to mask odor and unpleasant taste [30]. The sensitivity of Eudragit E 100 to change in pH is utilized in drug delivery systems because inflamed and cancerous tissues are characterized by a lower pH value [31,32]. This copolymer is mainly used as a coating material, nanocapsules, or nanoparticles. EE100 is also widely used to improve the solubility of drugs that are poorly soluble in water. The drug substance is then either dispersed in the biopolymer matrix or trapped in the nanocapsules [28,33–41].

Eudragit E 100 is often used as a blend with other biopolymers, which can result in the development of a new biopolymer with desired properties, such as a drug release profile. Farooq et al. produced Eudragit E 100/polycaprolactone microspheres in oil by the water solvent evaporation method [30]. Blended polylactic glycolic acid and Eudragit E 100 were proposed for the prevention of autoimmune diabetes [42]. There are many reports of the use of Eudragit E 100 in medicine, but few of them relate to bone implants.

There are several reports on the use of chitosan in combination with Eudragits. Vibhooti et al. developed Eudragit S 100-coated chitosan beads with pH-sensitivity for colon-targeted delivery [43]. Eudragit L 100 and S 100 were used for coating crosslinked chitosan microspheres with metronidazole by the emulsion solvent evaporation technique [44]. Interpolyelectrolyte complexes of chitosan and Eudragit L 100 were applied in oral controlled drug delivery systems [45]. Xu et al. prepared Eudragit L 100-coated mannosylated chitosan nanoparticles for oral bovine serum albumin delivery [46]. The addition of Eudragit RS to the pectin/chitosan films prepared by the casting/solvent evaporation method significantly decreased the swelling ratio of this polyelectrolyte complex in phosphate-buffered saline (PBS). Furthermore, the introduction of the Eudragit RS to the coating ensured a controllable slow release followed by a burst release of theophylline immediately after the change in pH [47]. Kouchak et al. revealed that increasing Eudragit's RL content in chitosan films could improve their mechanical properties without undesirable effects on their water uptake and oxygen penetration. The properties of these biopolymer coatings can be modified by changing the chitosan/Eudragit ratio [48].

The aim of this research is the electrophoretic deposition and characterization of the chit/EE100 coatings. According to the previous studies [47,48], the addition of Eudragit E 100 improves the mechanical properties of chitosan coatings and limits the dissolution rate of the chitosan coating at neutral pH. This type of coating may be a matrix for the controlled release of the drug used in the case of load-bearing implants. So far, there have been no reports in the literature regarding the production of this type of biopolymer coatings using the electrophoretic deposition method.

2. Materials and Methods

2.1. Materials

The Ti grade 2 (EkspresStal, Luboń, Poland) was used as a substrate. Table 1 shows its chemical composition given by the manufacturer. Commercial high molecular weight chitosan (high purity > 99%, *MW* ~ 310–375 kDa) coarse ground flakes and powder with a degree of deacetylation > 75% were purchased from Sigma-Aldrich (St. Louis, MO, USA). Eudragit E 100 granules (purity 99.9%, *MW* ~ 47 kDa) were provided by the Evonik Industries (Darmstadt, Germany). Acetic acid (99.9%) was obtained from Stanlab (Gliwice, Poland), while isopropanol (99.8%) and hydrochloric acid (30%) from POCH (Gliwice, Poland).

Table 1. The chemical composition of the Ti grade 2 substrate, wt.%.

Element	N	C	H	Fe	O	Ti
wt.%	0.009	0.013	0.001	0.168–0.179	0.190–0.170	remainder

2.2. Substrate Preparation

As a substrate, the Ti grade 2 round samples with a diameter of 12 mm and a height of 4 mm (cut from a rod) were used. All samples were wet ground using SiC abrasive papers up to grit #800. Prior to coating deposition, the Ti substrate was rinsed with isopropanol and distilled water.

2.3. Electrophoretic Deposition of Chitosan/Eudragit E 100 Coatings

Two different suspensions containing 0.25 g (suspension A) and 0.5 g (suspension B) of Eudragit E 100 were prepared for electrophoretic deposition. The appropriate amount of biopolymer was dissolved in 100 mL of 1% (*v*/*v*) aqueous acetic acid solution with 0.1 g of chitosan, according to the previous work [49]. This suspension was magnetically stirred (Dragon Lab MS-H-Pro+, Schiltigheim, France) for 24 h at room temperature.

Different time and deposition voltage values were used. The designation of samples with applied parameters is shown in Table 2. Ti substrate was used as a cathode, and the counter electrode was platinum mesh. The distance between electrodes connected to the DC power source (MCP/SPN110-01C, Shanghai MCP Corp., Shanghai, China) was about 10 mm. The deposition was carried out at room temperature. After deposition, the samples were rinsed with distilled water, dried at room temperature for 48 h, and stored in a desiccator for further characterization. After the deposition, the parameters ensuring the best quality of chit/EE100 coating were selected, and, for comparison, a chitosan coating without the addition of EE100 was prepared using these deposition parameters.

Table 2. Designations of experiment samples with the applied process parameters.

Suspension		Sample	Voltage (V)	Time (min)
A (0.25 g EE100)	100 mL of 1% (*v*/*v*) acetic acid with 0.1 g of chitosan	A1	10	1
		A3		3
		A1′	30	1
		A3′		3
B (0.5 g EE100)		B1	10	1
		B3		3
		B1′	30	1
		B3′		3

2.4. Structure and Morphology of Chitosan/Eudragit E 100 Coatings

The surfaces of the composite coating were examined using a high resolution scanning electron microscope (SEM JEOL JSM-7800 F, JEOL Ltd., Tokyo, Japan) with an LED detector at 5 kV acceleration voltage. Before testing, samples were sputtered with a 10 nm thick layer of gold using a

table-top DC magnetron sputtering coater (EM SCD 500, Leica, Vienna, Austria) in a pure Ar plasma condition (Argon, Air Products 99.999%). The surface roughness of all prepared samples was determined by using a contact profilometer with EVOVIS software (1.38.0.2) (Hommel Etamic Waveline, Jenoptik, Jena, Germany). The test was conducted according to the ISO 4287-1997 standard [50]. Three measurements were carried out for each sample, measurement distance was 8.8 mm with a scanning speed of 0.5 mm/s. Based on the tests, the average values of roughness (*Ra*), the peak-to-valley roughness (*Rz*), and maximum peak-to-mean height (*Rp*) were obtained. The qualitative elemental analysis of the obtained coatings was determined by the X-ray energy-dispersive spectrometer (EDS) (Edax Inc., Mahwah, NJ, USA). The X-ray diffraction spectroscopy (Phillips X'Pert Pro, Almelo, The Netherlands) was conducted (Cu Kα, λ = 0.1554 nm) in the 2θ range of 10°–90° at a 0.02 step and 2 s/point at ambient temperature and under atmospheric pressure. Fourier-transform infrared spectroscopy (FTIR, Perkin Elmer Frontier, Waltham, MA, USA) at a resolution of 2 cm^{-1} (scans number 32) in the range of 400–4000 cm^{-1} was utilized.

2.5. Mechanical Studies

Nanoindentation tests were performed using the NanoTest™ Vantage device (Micro Materials, Wrexham, Great Britain) with a Berkovich three-sided pyramidal diamond indenter. Ten independent measurements were performed for the Ti reference sample and the biopolymer coatings prepared at different deposition parameters. The distance between individual indents was 20 μm. The value of maximum force was 50 mN, the loading and unloading rate were set up at 20 s and the dwell period at maximum load was 10 s. The load–displacement curve was obtained for each measurement by the Oliver and Pharr method. Based on these curves, surface hardness (*H*) and Young's modulus (*E*) were determined. For the calculations, the values of Poisson's ratio 0.3 and 0.4 were used for the reference Ti sample and the samples with biopolymer coatings, respectively.

The scratch tests were carried out over a distance of 500 μm, the load increasing from 0 to 200 mN at a loading rate of 1.3 mN/s. The force that caused complete delamination of the coating from the substrate was determined based on an abrupt change in frictional force at the plot of the normal force versus friction force for each measurement. Besides, for its exact determination, all scratches were examined using an optical microscope (BX51, OLYMPUS, Tokyo, Japan).

2.6. Degradation Analysis

Dried and pre-weighed (Pioneer PA114CM/1, OHAUS, Greifensee, Switzerland) samples with chitosan and chit/EE100 coatings were immersed in artificial saliva solution (ASS, prepared according to reference [51]) at 37 °C temperature at different pH (3, 5, and 7) value for 1, 3 and 7 days. HCl was used to adjust the solution pH. According to reference [52], weight loss (*WL*) of the investigated coating was calculated as:

$$WL = \frac{W_1 - W_2}{W_1} \times 100\% \quad (1)$$

where W_1 is the weight of the dry sample with coating before swelling and W_2 is the weight of the dry sample after swelling. The measurement results were collected at an accuracy of 0.0001 g.

2.7. Corrosion Studies

The electrochemical measurements were made in a potentiodynamic mode in artificial saliva solution at 37 °C using a potentiostat/galvanostat (Atlas 0531, Atlas Sollich, Gdansk, Poland). A three-electrode cell setup was utilized, with platinum electrode as a counter electrode, and Ag/AgCl (saturated with potassium chloride) as a reference electrode. Before the experiment, the samples were stabilized at their open circuit potential (OCP) for 10 min. A potentiodynamic polarization test was conducted within a scan range −800/1000 mV at a potential change rate of 1 mV/s. Using the Tafel extrapolation method, the corrosion potential (E_{corr}) and corrosion current density (i_{corr}) values were determined.

2.8. Contact Angle Studies

The measurement of the water contact angle was carried out by falling drop method (Contact Angle Goniometer, Zeiss, Oberkochen, Germany) at room temperature and 10 s after drop out. The water drop volume was about 2 μL, and three measurements were performed for each sample.

3. Results and Discussion

3.1. Structure and Morphology of Chitosan/Eudragit E 100 Coatings

Figure 1 depicts the microstructure of the Ti grade 2 substrate, the chitosan coating, and the chit/EE100 coatings obtained by electrophoretic deposition. The Ti grade 2 substrate after wet grinding was characterized by a typical structure resulting from the grinding process [53]. The effects of EE100 content in the suspension, deposition time, and applied voltage on the quality of prepared coatings are visible. The increasing deposition time and the applied voltage resulted in more uneven coatings morphology. This effect has also been observed in other studies [54]. The increase in these parameters caused more rapid kinetics of coating deposition and bubble formation of hydrogen gas on the surface of the titanium sample caused by water electrolysis, which resulted in the deposition of a more heterogeneous coating [55,56]. The presence of hydrogen bubbles blocks the flow of biopolymer particles to the surface, which strongly affects the structure of coatings [57]. The prints of formedhydrogen bubbles are visible in the SEM images (Figure 1). In some areas of the coatings, it caused total exposure of the titanium substrate. The reduction in bubble formation can be achieved by reducing water content in the suspension by replacing it with, e.g., ethanol [58].

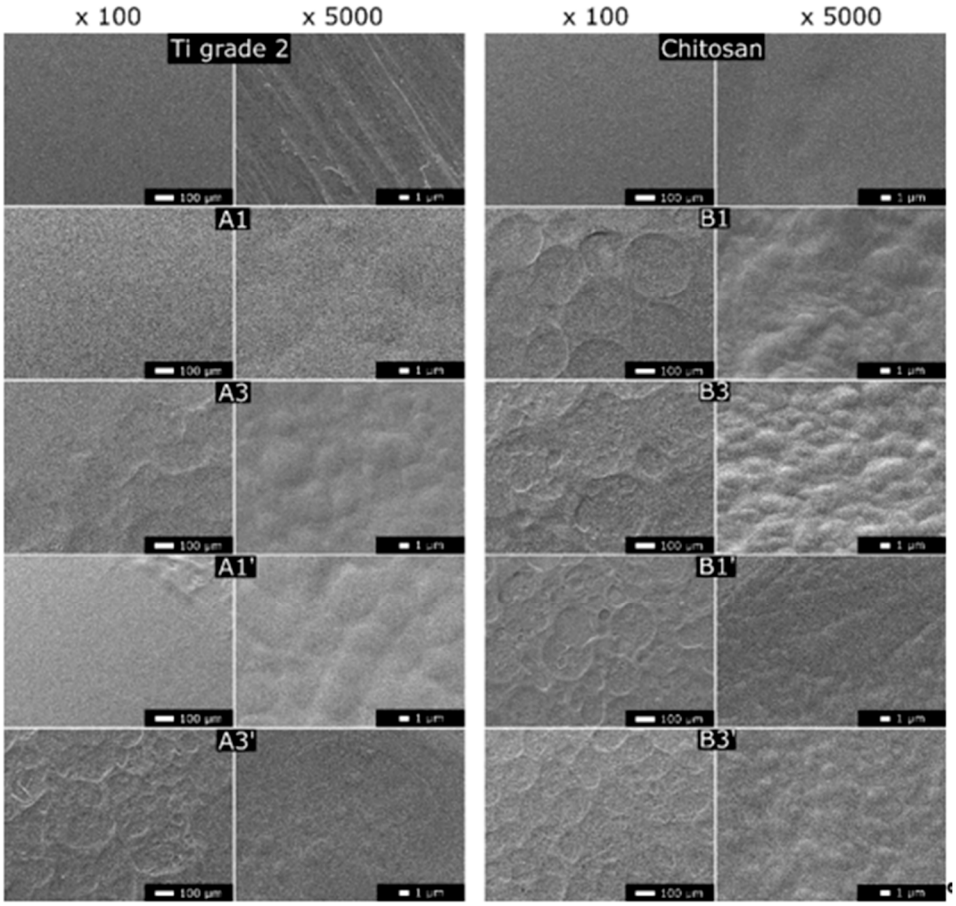

Figure 1. SEM images of the surface topography of the Ti grade 2 substrate, the chitosan coating, and the chit/EE100 coatings obtained at different deposition parameters; the images obtained at different magnifications, ×100 (on the left) and ×5000 (on the right).

An increase in the content of EE100 in the suspension also contributed to the increase in heterogeneity of the obtained coatings. Similar to other biopolymer coatings, an increase in Eudragit content in the suspension caused a disturbance in particle flow, resulting in a more porous coating [59]. For all chit/EE100 samples, the images obtained at higher magnifications showed a microporous structure of the coatings. However, it has been reported that the porosity of implant coatings promotes in vivo cell growth [23]. The A1 sample, prepared at the lowest deposition parameters, showed the highest homogeneity. In this case, the coating completely covered the titanium substrate surface, and the images obtained at higher magnifications revealed slight unevenness. Therefore, the A1 sample was selected for the next examinations. For comparison purposes, using the A1 sample deposition parameters, a chitosan coating without the addition of EE100 was prepared for the remaining tests. Continuous coating was observed, and it was characterized by uniformly distributed unevenness visible at higher magnifications. Compared to the A1 sample, a similar homogeneity was observed. The mechanism of creating chitosan coatings most likely involves loss of charge in the high pH value, an alkaline region on the cathode surface by chitosan protonated amino groups, and the formation of insoluble precipitates [60].

Table 3 summarizes the mean values of surface roughness parameters: the average roughness (*Ra*), the peak-to-valley roughness (*Rz*), and maximum peak-to-mean height (*Rp*) obtained for the Ti grade 2 substrate, the chitosan coating, and the chit/EE100 coatings.

Table 3. Surface roughness parameters of the Ti grade 2 substrate, the chitosan coating, and the chit/EE100 coatings (mean ± SD; $n = 3$).

Surface Roughness Parameters (μm)			
Sample	***Ra***	***Rz***	***Rp***
Ti grade 2	0.12 ± 0.01	0.77 ± 0.13	0.44 ± 0.11
Chitosan	0.15 ± 0.05	1.34 ± 0.58	0.88 ± 0.46
A1	1.57 ± 0.05	7.01 ± 0.44	4.29 ± 0.29
A3	2.84 ± 0.11	11.39 ± 0.05	6.31 ± 0.11
A1′	4.63 ± 0.68	20.27 ± 2.05	10.24 ± 1.00
A3′	2.98 ± 0.24	14.48 ± 0.56	8.01 ± 0.37
B1	2.53 ± 0.47	12.16 ± 1.97	7.64 ± 1.65
B3	2.66 ± 0.31	12.47 ± 1.29	7.70 ± 1.24
B1′	2.39 ± 0.11	11.76 ± 0.64	7.28 ± 0.71
B3′	2.93 ± 0.38	12.92 ± 1.28	7.19 ± 0.88

The titanium substrate showed the lowest roughness. The deposition of biopolymer coatings by the electrophoretic method resulted in increased surface roughness compared to a bare substrate. A similar relationship was observed in previous studies [49]. The chitosan coating showed roughness similar to the substrate after grinding; in the case of chit/EE100 coatings, a significant increase in mean values of parameters *Ra*, *Rz*, and *Rp* was observed. The reason for this lies in the more rapid EPD process for chit/EE100 deposition and the formation of hydrogen bubbles on the cathode [55]. The results obtained are consistent with the SEM images shown in Figure 1. Increased surface roughness allows for better tissue adhesion and stabilization of the implant in the initial phase [61].

Figure 2 presents the results of the EDS measurements for the Ti grade 2 substrate, the sample with chitosan coating, and the sample with chit/EE100 coating (sample A1). This analysis was only qualitative. The samples previously subjected to SEM examinations were used; hence, peaks referring to Au were visible in all spectra. EDS spectrum of the substrate confirmed the presence of Ti. For the other two samples, peaks related to Ti were less intense. Moreover, constituents of the coatings (O, C) and Ti element from substrate were noted; however, Ti peaks were less sharp. In the case of the chit/EE100 sample, the Ti peaks reached a lower intensity compared to the chitosan coating, which could result from a greater thickness of the chit/EE100 coating. The addition of Eudragit E 100 to the chitosan coating reduced the intensity of the O peak. This oxygen decrease is difficult to explain. Presumably, the porous chitosan coatings contain a lot of molecular oxygen, and the addition of Eudragit may be placed inside the empty spaces at the expense of oxygen. The spectra obtained

confirmed the absence of other elements in the prepared samples, indicating no contamination during the EPD process.

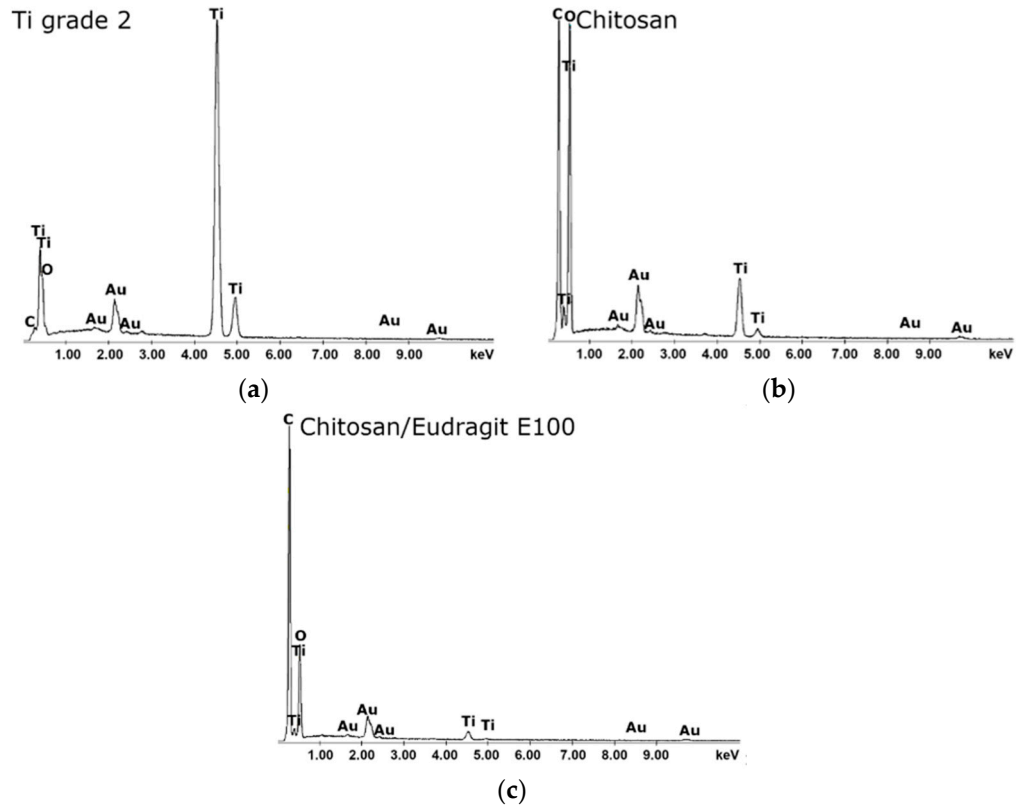

Figure 2. X-ray energy dispersion spectroscopy spectra of the Ti grade 2 substrate (**a**), the sample with the chitosan coating (**b**), and (**c**) sample with chitosan/Eudragit E 100 coating (A1 sample).

Figure 3a depicts the X-ray diffractograms of analyzed specimens. Within the patterns, only peaks associated with the titanium alpha phase can be identified (JCPDS file 44-1294), which indicates the relatively thin, both chitosan and chit/EE100, layers. No reflections of chitosan or Eudragit E 100 can be indexed within the obtained patterns [62,63].

Figure 3b presents the FTIR results of measured samples. In the case of the spectra acquired for the layered chitosan samples, some low-intensity bands were observed. These bands can be attributed to the chitosan layer. The clear bands which appear in the range of 1680–1480 cm^{-1} can be associated with the vibrations of carbonyl bonds (C=O) of the amide groups, when absorption in the range from 1160 to 1000 cm^{-1} can be recognized as vibrations of CO bonds [64]. In the case of the spectra recorded for the sample with chit/EE100, the bands with higher intensity are visible. FTIR spectrum of Eudragit E 100 presented typical bands of ester groups in the range of 1300–1150 cm^{-1}. A strong C=O ester stretching band was observed at 1720 cm^{-1}. In addition, vibrations of the hydrocarbon chain were observed at 1385, 1450–1490, and 2950 cm^{-1}. Signals visible between 2770 and 2820 cm^{-1} can, on the other hand, be attributed to dimethylethanolamine (DMAE) groups. Such bands were already observed for the stand-alone Eudragit E 100 polymer [65].

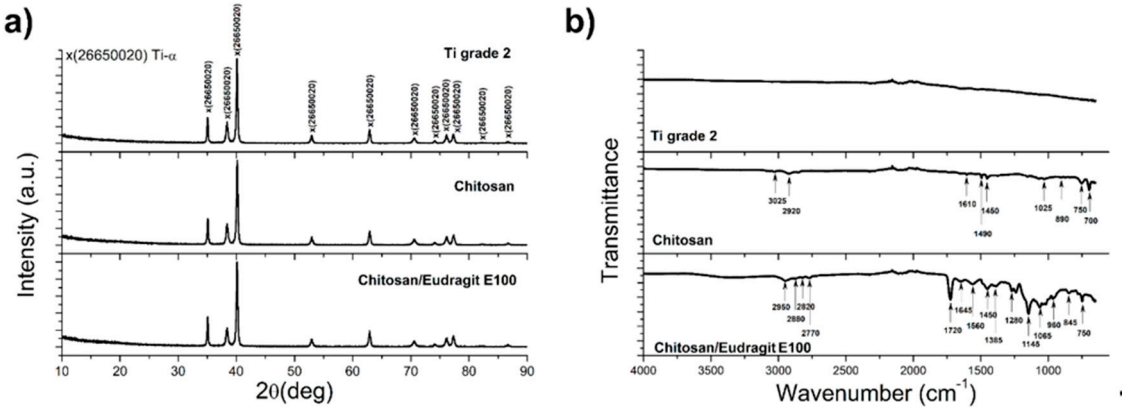

Figure 3. (**a**) X-ray diffractograms and (**b**) FTIR spectra of the Ti grade 2 substrate, the chitosan coating, and the chit/EE100 coating (A1 sample).

3.2. Mechanical Studies

For long-term and load-bearing implants, the mechanical properties are among the most significant factors determining implant durability. The difference between the properties of human bone and the implant can lead to loosening of the implant [66]. Nanoindentation is an increasingly used method for testing thin coatings for biomedical applications [67]. This technique allows for making indents with sizes measured in nanometers, which permits testing thin coatings. It enables the determination of mechanical parameters such as hardness and Young's modulus, and nanoindentation properties: maximum depth of indentation, plastic, and elastic work.

Figure 4 presents single hysteresis load-deformation graphs for the substrate and the prepared coatings. Each of the curves consists of three sections: increasing the force to the maximum value, holding with maximum force, and offloading. A slight deflection on the deformation curves is visible for all tested samples, which results from the temperature drift during the measurement. Based on the obtained curves, nanoindentation parameters were calculated, as presented in Figure 5.

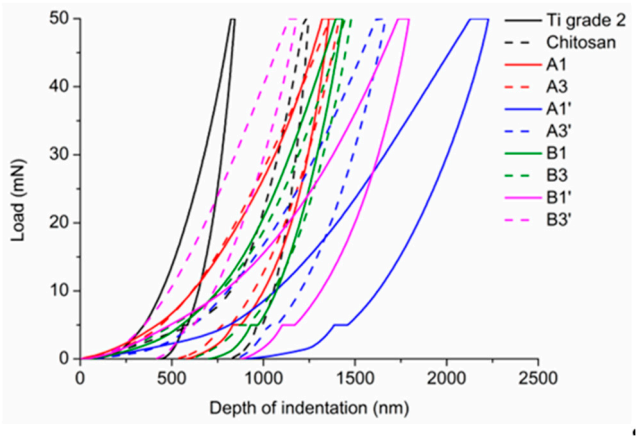

Figure 4. Hysteresis plots of load-deformation for a single indentation measurement for the Ti grade 2 substrate, chitosan, and chit/EE100 coatings.

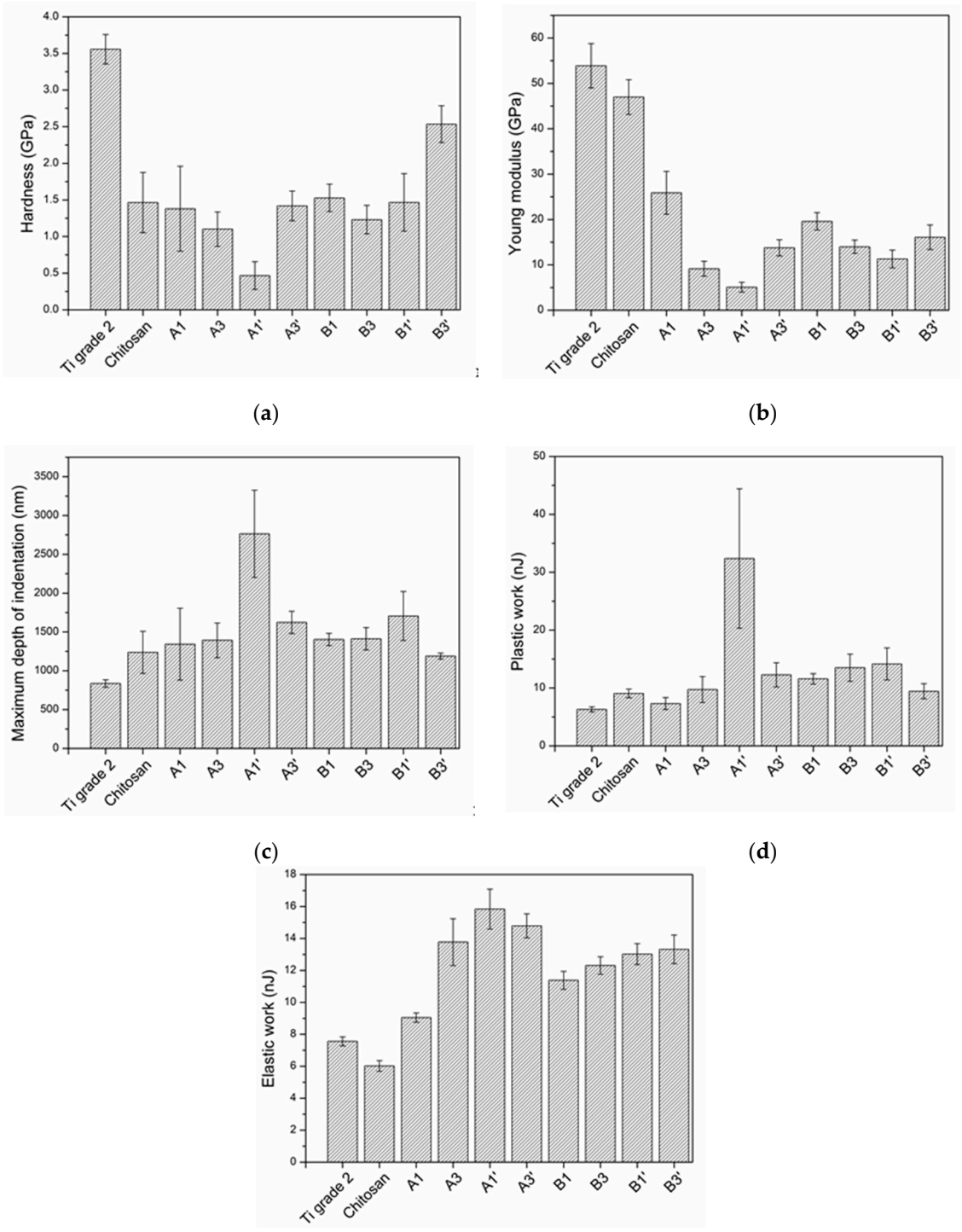

Figure 5. Mechanical properties: (**a**) hardness and (**b**) Young's modulus; nanoindentation properties: (**c**) maximum depth of indentation, (**d**) plastic work and (**e**) elastic work for the Ti grade 2 substrate, the chitosan coating, and the chit/EE100 coatings. Data are presented as the mean ± SD (n = 10).

The Ti grade 2 substrate showed the highest hardness and Young's modulus, which resulted in the smallest indentation depth obtained. All coated samples showed worse mechanical properties, but higher nanoindentation properties as compared to the Ti grade 2 substrate. Similar relationships were observed in the past studies, and they result from the features, like chemical bonds, of the specific material groups. Metals show higher mechanical properties compared to polymers, which leads to a lower depth of indentation [49,68]. In the case of the chitosan coating, the obtained values of hardness and Young's modulus were similar to the values presented in the previous work [49].

Coatings containing EE100 had similar hardness (except A1′ and B3′) and much lower Young's modulus compared to that of the chitosan coating. This can be explained by the different thickness, packing density, and porosity of chit/EE100 coatings compared to a no-Eudragit coating. The highest hardness of sample B3′ results from the application of the highest deposition parameters (time, voltage, EE100 concentration). This coating was probably the thickest and most densely packed. For sample A1′, the lowest hardness value may be due to the thinnest coating and low packing density, due to the short deposition time and lower EE100 concentration in the suspension [69]. The Young's modulus values of chit/EE100 coatings were similar to the value of Young's modulus of human bones. The Young's modulus value closest to Young's modulus of the human tibia cortical bone (E = 25.8 GPa) was obtained for sample A1 [70]. This coating showed the highest homogeneity. In implantology, there must be no significant differences in the mechanical properties between the implant and the human bone [66]. The obtained values of parameters determining the mechanical properties of coatings could be influenced by the titanium substrate.

It was difficult to determine the effect of applied coating deposition parameters on the mechanical properties of the prepared coatings. However, for coatings deposited at 10 V, the longer deposition time resulted in a decrease in the hardness and Young's modulus of the coatings. An inverse relationship was observed for 30 V. An increase in the concentration of EE100 in the suspension increased the hardness of the coatings. According to the SEM images (Figure 1), deposition kinetics increased with increased applied voltage, resulting in a more heterogeneous coating structure with visible chit/EE100 clusters that could increase the hardness of coatings locally [71].

The value of elastic work for a particular sample exceeded the value of plastic work. For all samples, the value of plastic work increased with an increased maximum depth of indentation. The obtained results confirm that the tested coatings are more elastic (less brittle) than the reference chitosan coatings, which is a positive impact of Eudragit addition. The increase in plastic work with increasing indent depth results from increasing plastic deformation at the tip, a number of dislocations, and plastic strengthening. High values of standard deviations from the average values probably result from the heterogeneity of the coatings produced as a result of bubble formation during the EPD process [49,58]. There are reports in the literature on a wide range of hardness, Young's modulus, and nanoindentation parameters for chitosan coatings. It results from the differences in applied conditions and measurement parameters [72–74]. Fahim et al. and Akhtar et al. applied much lower loads during the indentation measurements, 3 and 5 mN, respectively, obtaining much lower hardness values of chitosan coatings. Possibly, a too high preliminary load was applied in the case of the conducted tests, and therefore, the results were influenced by the titanium substrate [73,74]. There is no information concerning the mechanical properties of chit/EE100 coatings.

Figure 6 presents plots of the dependence of the friction force on the normal force for each sample with an indication of the critical force causing complete delamination of the coating from the titanium substrate. The value of the critical force was determined based on a comparison of the frictional force dependence on the normal force and optical microscopic observation of the made scratch.

Table 4 shows the values of the average critical load force (Lc) and the corresponding friction force (Lf) determined from scratch test measurements. All coatings with Eudragit E 100 showed higher adhesion to the titanium substrate compared to the chitosan coating. This may be attributed to an increase in the density of chitosan coatings due to the addition of Eudragit E 100 [48]. The most increased adhesion was demonstrated for the A3 and B3 samples. These coatings were prepared at a lower voltage, which resulted in gentle kinetics of biopolymer particle deposition and the formation of a densely packed coating [75]. The effect of the deposition parameters on the critical friction and load is poorly visible. However, there was a tendency (except for samples B1′ and B3′) that the values of Lc and Lf increased with increasing deposition time. This is probably due to the increase in the thickness of the biopolymer coating. The high values of standard deviations were due to the heterogeneity of the produced coatings. High adhesion of the coating to the implant surface is an important factor during the implant placement procedure, as the implant is exposed to heavy loads that can lead to the removal of the coating [76]. There are almost no studies on the adhesion of

chitosan and chit/EE100 coatings to metallic substrates in the literature. Therefore, our data, relating to composite coatings containing chitosan, are difficult to compare [49,77].

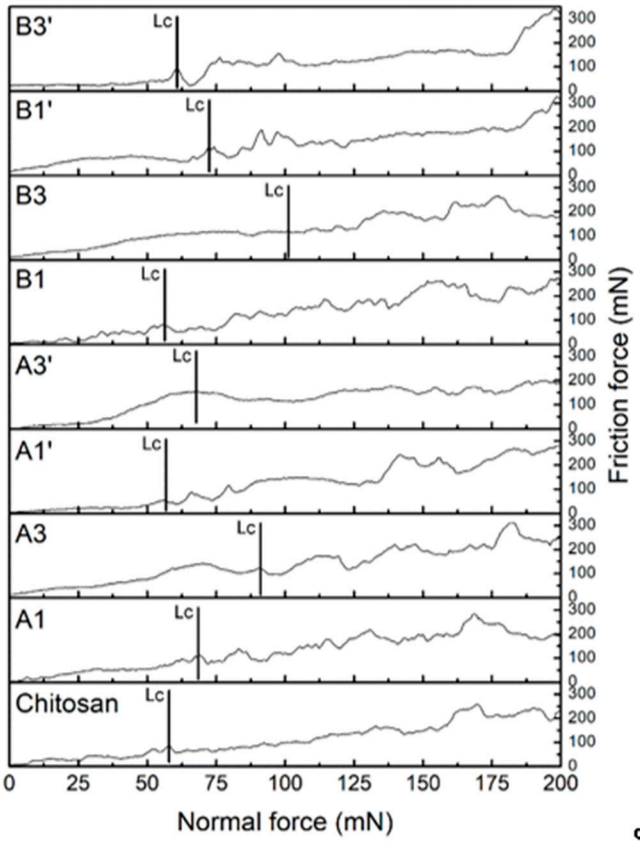

Figure 6. The dependence of the friction force on the normal force obtained for chitosan and chitosan/Eudragit E100 coatings with an indication of the critical force causing complete delamination of the coating from the titanium substrate.

Table 4. Nanoscratch test properties of the chitosan and chitosan/Eudragit E 100 coatings (mean ± SD; $n = 10$).

Nanoscratch Test Properties		
Sample	**Critical Load, *Lc* (mN)**	**Critical Friction, *Lf* (mN)**
Chitosan	53.87 ± 22.04	61.24 ± 22.04
A1	64.24 ± 25.91	90.73 ± 30.95
A3	91.28 ± 23.06	126.66 ± 46.53
A1′	58.05 ± 8.59	70.28 ± 22.79
A3′	68.18 ± 25.10	105.87 ± 44.77
B1	56.42 ± 23.82	83.34 ± 32.18
B3	90.63 ± 37.58	115.86 ± 48.16
B1′	73.88 ± 15.58	96.55 ± 25.55
B3′	61.00 ± 16.80	84.68 ± 34.24

3.3. Degradation Analysis

The test results of the degradation rate of the investigated coatings are shown in Figure 7. The impact of exposure time and pH on weight loss is visible for both tested samples. The degree of degradation of both the chitosan coating and the chit/EE100 coating increased with the increase in the exposure time and the decrease in the pH of the environment. Similar correlations were reported in other works [78]. Under the influence of lowered pH, the protonation of chitosan and EE100 amine groups intensifies, and as a result of repulsive interaction, the degradation occurs [79,80]. The chit/EE100 coating is significantly more stable at a pH of 7 compared to the coating without Eudragit.

The mass loss after 7 days at pH 7 was 1.79% and 32%, respectively. However, the chit/EE100 coating showed greater sensitivity to pH changes. Lowering the pH to 5 caused a sharp increase in the mass loss. The degradation of the coating was comparable at pH 5 and 3. The degradation of the chitosan coating with a decrease in pH was smoother. The chit/EE100 blend contains more amine groups in comparison to chitosan alone. Therefore, the pH reduction results in stronger repulsion of the polymer chains during protonation, resulting in more rapid degradation of the coating [80].

Due to the high stability at neutral pH and high sensitivity to its decline, coatings based on chitosan and Eudragit E 100 could be used in controlled drug delivery systems [81]. The use of this type of biopolymer with, e.g., silver nanoparticles as a coating for implants, would protect against the development of bacterial infection after implantation [82]. Such a system could provide controlled release of the drug substance only at the time of inflammation, which is associated with a decrease in the pH of peri-implant tissues [79]. The high stability of the chit/EE100 coating at neutral pH would also significantly reduce the adverse effect of burst release, i.e., the rapid release of a large dose of the drug after the implant has been placed in an environment simulating body fluids [83].

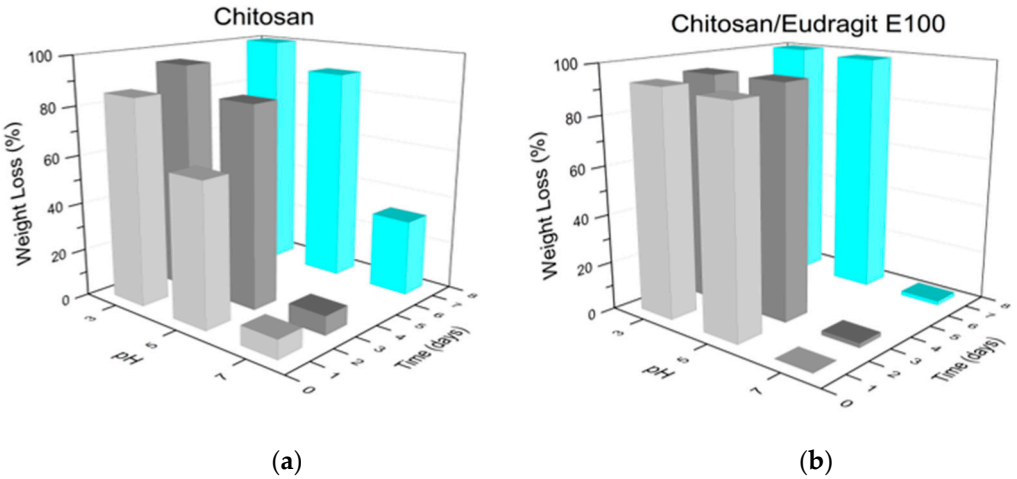

(**a**) (**b**)

Figure 7. Results of the weight loss (WL) analysis of the chitosan and chit/EE100 coating (A1 sample).

3.4. Corrosion Studies

Figure 8 depicts potentiodynamic polarization curves obtained for the uncoated Ti grade 2 substrate and chitosan, and chit/EE100 coatings in ASS at 37 °C temperature. Table 5 summarizes the determined corrosion parameters such as open circuit potential, corrosion potential, and current density. Moreover, Figure 9 shows SEM images of the surface topography of the Ti grade 2 substrate, the chitosan coating, and the chit/EE100 coating obtained after corrosion studies. According to the results, samples with coatings showed higher corrosion resistance as measured by corrosion current density compared to the bare Ti grade 2 specimen. Chitosan-based coatings formed a protective layer separating the metallic substrate from the corrosive environment [16]. The addition of EE100 to the chitosan coating slightly reduced its corrosion resistance. This results from a more heterogeneous structure of the chit/EE100 coating and therefore, reduced barrier properties (Figure 9). In the case of samples with coatings, the corrosion potential value was shifted towards positive values compared to the uncoated sample. A slight shift of corrosion potential can be attributed, as confirmed by Tafel curves, to the change of activation polarization, i.e., runs of cathodic and anodic parts. Despite that, the deep decrease in corrosion current can be ascribed mainly to the increasing ohmic resistance of the biopolymer coating as compared to the metallic substrate [55]. Improvement of corrosion resistance of the metallic substrate after application of the chitosan coating was observed in other studies [55,84]. The corrosion resistance of metal implants is crucial because it can affect biocompatibility and mechanical integrity [85]. Implants in aggressive environments are particularly susceptible to corrosion [86]. Titanium is stable in a neutral, alkaline, and only slightly acidic environment; below pH ~ 5, it starts to dissolve. In addition, local pH reduction in peri-implant

tissues occurs during inflammation in the human body [87,88]. In such conditions, corrosion products can penetrate peri-implant tissues, which can lead to metallosis and implant rejection [89].

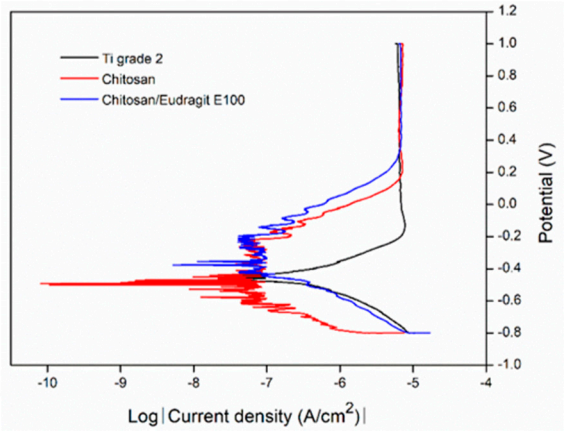

Figure 8. Potentiodynamic polarization curves of uncoated Ti grade 2 substrate, chitosan, and chit/EE100 (A1 sample) coatings in ASS at 37 °C temperature.

Table 5. Open circuit potential, corrosion potential, and current density of the Ti grade 2 substrate and coated substrate with chitosan and chit/EE100 (sample A1).

Sample	OCP (V)	E_{corr} (V)	i_{corr} (nA/cm²)
Ti grade 2	−0.471	−0.453	794.15
Chitosan	−0.351	−0.445	4.79
Chitosan/EE100 (A1 sample)	−0.306	−0.315	93.79

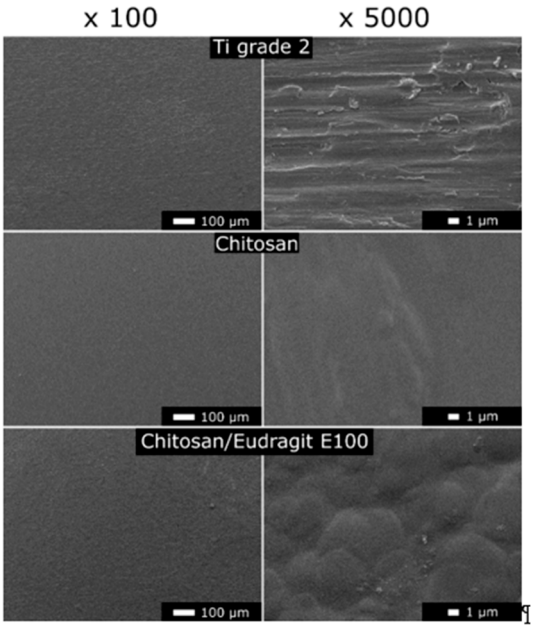

Figure 9. SEM images of the surface topography of the Ti grade 2 substrate, the chitosan coating, and the chit/EE100 coating obtained after corrosion studies; the images obtained at different magnifications, ×100 (on the left) and ×5000 (on the right).

3.5. Contact Angle Studies

Figure 10 shows the values of the average contact angle for the reference Ti grade 2 sample and samples with chitosan and chit/EE100 coatings. The obtained results confirmed the hydrophilic character of all the tested samples. Due to a more uneven surface, almost all samples (except A1')

showed a lower contact angle compared to the reference sample Ti grade 2. The addition of EE100 reduced the wettability of the coating. However, the contact angle was less than 90°. The EE100 coating is water-repellent [62]. The obtained results did not reveal the relationship between the concentration of EE100 in the suspension, the deposition time, or the value of applied voltage and the value of the contact angle. For samples with coatings, a higher surface roughness results in a higher wetting angle. In some cases, surfaces considered to be more uneven were more hydrophilic, probably due to the penetration of water into the irregularities of the coatings [90]. Some studies suggested that for the best cell adhesion, the contact angle of the coatings should be in the range of 40°–60°. However, this range depends on the type of cell and may vary [91]. In the case of bone cells, this range is given as 35°–85°, and the optimum value is 55° [92]. Therefore, all tested samples were close to the upper limit of this requirement.

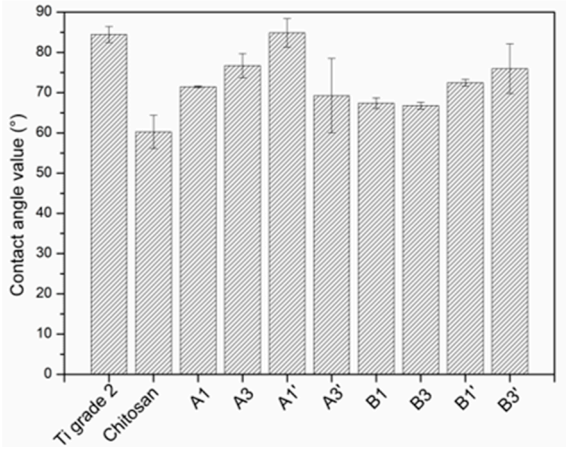

Figure 10. The water contact angle for the Ti grade 2 substrate, the chitosan coating, and the chit/EE100 coatings; data are presented as the mean ± SD (n = 3).

4. Conclusions

The obtained results confirm that it is possible to produce chitosan coatings with the addition of Eudragit E 100 in a one-stage electrophoretic deposition process. Applied deposition parameters affect the quality of the obtained coatings. The increase in the concentration of EE100, voltage, and time of deposition resulted in a more heterogeneous structure of the coatings. The best process deposition parameters for chit/EE100 coating on the surface of Ti grade 2 substrate are the 2.5 g/L of EE100 and 1 g/L of high weight chitosan with the degree of deacetylation > 75 % of 1% (v/v) of the aqueous acetic acid solution, EPD voltage 10 V and EPD time 1 min at room temperature.

Compared to the chitosan coating, the chit/EE100 coatings showed similar hardness and significantly lower Young's modulus, similar to that of a human cortical bone; improved adhesion of the coating to the titanium substrate; a much lower degradation rate at neutral pH. The corrosion resistance and wettability of these coatings were comparable.

The successful deposition of this biopolymer coating, susceptible to pH change, forms a good platform for controlled drug delivery systems, where the antibacterial vector can be silver nanoparticles dispersed in the biopolymer matrix. The production of such a composite coating based on chitosan, EE100, and silver nanoparticles will be the subject of further research. It would be possible to use them as a coating containing a drug substance, e.g., on load-bearing implants, which could limit the adverse effects of the peri-implantitis phenomenon.

Author Contributions: Conceptualization, Ł.P., M.B., and A.Z.; methodology, Ł.P., M.B., A.M.-G., G.S., and M.J.; formal analysis, Ł.P., M.B., A.Z., and A.M.-G.; investigation, Ł.P., M.B., A.M.-G., G.S., and M.J.; writing—original draft preparation, Ł.P., M.B., and A.Z.; writing—review and editing, Ł.P., M.B., and A.Z.; supervision, M.B. and A.Z. All authors have read and agree to the published version of the manuscript.

Funding: This research received no external funding.

Acknowledgments: The authors of the manuscript would like to thank Evonik Industries (Darmstadt, Germany) for the donation of material used for experiments and Robert Kozioł from the Department of Applied Physics and Mathematics, the Gdansk University of Technology for technical assistance in samples preparation.

Conflicts of Interest: The authors declare no conflict of interest.

References.

1. Prasad, S.; Ehrensberger, M.; Gibson, M.P.; Kim, H.; Monaco, E.A. Biomaterial properties of titanium in dentistry. *J. Oral Biosci.* **2015**, *57*, 192–199.
2. Assis, S.L.; Wolynec, S.; Costa, I. The electrochemical behaviour of Ti-13Nb-13Zr alloy in various solutions. *Mater. Corros.* **2008**, *59*, 739–743.
3. Niemeyer, T.C.; Grandini, C.R.; Pinto, L.M.C.; Angelo, A.C.D.; Schneider, S.G. Corrosion behavior of Ti-13Nb-13Zr alloy used as a biomaterial. *J. Alloys Compd.* **2009**, *476*, 172–175.
4. Liu, X.; Chu, P.K.; Ding, C. Surface modification of titanium, titanium alloys, and related materials for biomedical applications. *Mater. Sci. Eng. R Rep.* **2004**, *47*, 49–121.
5. Rau, J.V.; Fosca, M.; Cacciotti, I.; Laureti, S.; Bianco, A.; Teghil, R. Nanostructured Si-substituted hydroxyapatite coatings for biomedical applications. *Thin Solid Films* **2013**, *543*, 167–170.
6. Souza, J.C.M.; Sordi, M.B.; Kanazawa, M.; Ravindran, S.; Henriques, B.; Silva, F.S.; Aparicio, C.; Cooper, L.F. Nano-scale modification of titanium implant surfaces to enhance osseointegration. *Acta Biomater.* **2019**, *94*, 112–131.
7. Mistry, S.; Kundu, D.; Datta, S.; Basu, D. Comparison of bioactive glass coated and hydroxyapatite coated titanium dental implants in the human jaw bone. *Aust. Dent. J.* **2011**, *56*, 68–75.
8. Schmaljohann, D. Thermo- and pH-responsive polymers in drug delivery. *Adv. Drug Deliv. Rev.* **2006**, *58*, 1655–1670.
9. Sponchioni, M.; Capasso Palmiero, U.; Moscatelli, D. Thermo-responsive polymers: Applications of smart materials in drug delivery and tissue engineering. *Mater. Sci. Eng. C* **2019**, *102*, 589–605.
10. Wen, J.; Lei, J.; Chen, J.; Gou, J.; Li, Y.; Li, L. An intelligent coating based on pH-sensitive hybrid hydrogel for corrosion protection of mild steel. *Chem. Eng. J.* **2020**, *392*, 123742.
11. Zhang, A.; Jung, K.; Li, A.; Liu, J.; Boyer, C. Recent advances in stimuli-responsive polymer systems for remotely controlled drug release. *Prog. Polym. Sci.* **2019**, *99*, 101164.
12. Fu, X.; Hosta-Rigau, L.; Chandrawati, R.; Cui, J. Multi-stimuli-responsive polymer particles, films, and hydrogels for drug delivery. *Chem* **2018**, *4*, 2084–2107.
13. Kofuji, K.; Qian, C.J.; Nishimura, M.; Sugiyama, I.; Murata, Y.; Kawashima, S. Relationship between physicochemical characteristics and functional properties of chitosan. *Eur. Polym. J.* **2005**, *41*, 2784–2791.
14. Nikam, V. Eudragit a versatile polymer: A review. *Pharmacologyonline* **2011**, *1*, 152–164.
15. Muxika, A.; Etxabide, A.; Uranga, J.; Guerrero, P.; de la Caba, K. Chitosan as a bioactive polymer: Processing, properties and applications. *Int. J. Biol. Macromol.* **2017**, *105*, 1358–1368.
16. Simchi, A.; Pishbin, F.; Boccaccini, A.R. Electrophoretic deposition of chitosan. *Mater. Lett.* **2009**, *63*, 2253–2256.
17. Ahmad, M.; Manzoor, K.; Singh, S.; Ikram, S. Chitosan centered bionanocomposites for medical specialty and curative applications: A review. *Int. J. Pharm.* **2017**, *529*, 200–217.
18. Ali, A.; Ahmed, S. A review on chitosan and its nanocomposites in drug delivery. *Int. J. Biol. Macromol.* **2018**, *109*, 273–286.
19. Ahmed, S.; Ikram, S. Chitosan based scaffolds and their applications in wound healing. *Achiev. Life Sci.* **2016**, *10*, 27–37.
20. Farrokhi-Rad, M.; Shahrabi, T.; Mahmoodi, S.; Khanmohammadi, S. Electrophoretic deposition of hydroxyapatite-chitosan-CNTs nanocomposite coatings. *Ceram. Int.* **2017**, *43*, 4663–4669.
21. Ordikhani, F.; Simchi, A. Long-term antibiotic delivery by chitosan-based composite coatings with bone regenerative potential. *Appl. Surf. Sci.* **2014**, *317*, 56–66.
22. Park, J.H.; Saravanakumar, G.; Kim, K.; Kwon, I.C. Targeted delivery of low molecular drugs using chitosan and its derivatives. *Adv. Drug Deliv. Rev.* **2010**, *62*, 28–41.
23. Jiang, T.; Zhang, Z.; Zhou, Y.; Liu, Y.; Wang, Z.; Tong, H.; Shen, X.; Wang, Y. Surface functionalization of titanium with chitosan/gelatin via electrophoretic deposition: Characterization and cell behavior. *Biomacromolecules* **2010**, *11*, 1254–1260.

24. Luo, X.L.; Xu, J.J.; Wang, J.L.; Chen, H.Y. Electrochemically deposited nanocomposite of chitosan and carbon nanotubes for biosensor application. *Chem. Commun.* **2005**, *16*, 2169–2171.
25. Wang, Y.; Guo, X.; Pan, R.; Han, D.; Chen, T.; Geng, Z.; Xiong, Y.; Chen, Y. Electrodeposition of chitosan/gelatin/nanosilver: A new method for constructing biopolymer/nanoparticle composite films with conductivity and antibacterial activity. *Mater. Sci. Eng. C* **2015**, *53*, 222–228.
26. Franco, P.; de Marco, I. Eudragit: A novel carrier for controlled drug delivery in supercritical antisolvent coprecipitation. *Polymers (Basel)* **2020**, *12*, 234.
27. Moustafine, R.I.; Kemenova, V.A.; Van den Mooter, G. Characteristics of interpolyelectrolyte complexes of Eudragit E 100 with sodium alginate. *Int. J. Pharm.* **2005**, *294*, 113–120.
28. Doerdelmann, G.; Kozlova, D.; Epple, M. A pH-sensitive poly(methyl methacrylate) copolymer for efficient drug and gene delivery across the cell membrane. *J. Mater. Chem. B* **2014**, *2*, 7123–7131.
29. Leopold, C.S.; Eikeler, D. Eudragit® E as coating material for the pH-controlled drug release in the topical treatment of inflammatory bowel disease (IBD). *J. Drug Target.* **1998**, *6*, 85–94.
30. Farooq, U.; Khan, S.; Nawaz, S.; Ranjha, N.M.; Haider, M.S.; Khan, M.M.; Dar, E.; Nawaz, A. Enhanced gastric retention and drug release via development of novel floating microspheres based on Eudragit E 100 and polycaprolactone: Synthesis and in vitro evaluation. *Des. Monomers Polym.* **2017**, *20*, 419–433.
31. Świeczko–Żurek, B.; Bartmański, M. Investigations of titanium implants covered with hydroxyapatite layer. *Adv. Mater. Sci.* **2016**, *16*, 78–86.
32. Cometa, S.; Bonifacio, M.A.; Mattioli-Belmonte, M.; Sabbatini, L.; De Giglio, E. Electrochemical strategies for titanium implant polymeric coatings: The why and how. *Coatings* **2019**, *9*, 268.
33. Chaurasia, S.; Chaubey, P.; Patel, R.R.; Kumar, N.; Mishra, B. Curcumin-polymeric nanoparticles against colon-26 tumor-bearing mice: Cytotoxicity, pharmacokinetic and anticancer efficacy studies. *Drug Dev. Ind. Pharm.* **2015**, *42*, 694–700.
34. Selvan, K.; Mohanta, G.; Manna, P.K. Solid-phase preparation and characterization of albendazole solid dispersion. *Ars Pharm.* **2006**, *47*, 91–107.
35. Valizadeh, H.; Zakeri-Milani, P.; Barzegar-Jalali, M.; Mohammadi, G.; Danesh-Bahreini, M.A.; Adibkia, K.; Nokhodchi, A. Preparation and characterization of solid dispersions of piroxicam with hydrophilic carriers. *Drug Dev. Ind. Pharm.* **2007**, *33*, 45–56.
36. Joshi, G.V.; Kevadiya, B.D.; Bajaj, H.C. Controlled release formulation of ranitidine-containing montmorillonite and Eudragit® E-100. *Drug Dev. Ind. Pharm.* **2010**, *36*, 1046–1053.
37. Goddeeris, C.; Willems, T.; Houthoofd, K.; Martens, J.A.; Van den Mooter, G. Dissolution enhancement of the anti-HIV drug UC 781 by formulation in a ternary solid dispersion with TPGS 1000 and Eudragit E100. *Eur. J. Pharm. Biopharm.* **2008**, *70*, 861–868.
38. Elgindy, N.; Samy, W. Evaluation of the mechanical properties and drug release of cross-linked Eudragit films containing metronidazole. *Int. J. Pharm.* **2009**, *376*, 1–6.
39. Nguyen, C.A.; Konan-kouakou, Y.N.; Allémann, E.; Doelker, E.; Quintanar-guerrero, D.; Fessi, H.; Gurny, R. Preparation of surfactant-free nanoparticles of methacrylic acid copolymers used for film coating. *AAPS PharmSciTech* **2006**, *7*, 63–70.
40. Lin, S.; Chen, K.; Run-chu, L. Design and evaluation of drug-loaded wound dressing having thermoresponsive, adhesive, absorptive and easy peeling properties. *Biomaterials* **2001**, *22*, 2999–3004.
41. Prabhushankar, G.L.; Gopalkrishna, B.; Manjunatha, K.M.; Girisha, C.H. Formulation and evaluation of Levofloxacin dental films for periodontitis. *Int. J. Pharm. Pharm. Sci.* **2010**, *2*, 162–168.
42. Basarkar, A.; Singh, J. Poly(lactide-co-glycolide)-polymethacrylate nanoparticles for intramuscular delivery of plasmid encoding interleukin-10 to prevent autoimmune diabetes in mice. *Pharm. Res.* **2009**, *26*, 72–81.
43. Vibhooti, P.; Rajan, G.; Seema, B. Eudragit and chitosan—The two most promising polymers for colon drug delivery. *Int. J. Pharm. Biol. Arch.* **2013**, *4*, 399–410.
44. Chourasia, M.K.; Jain, S.K. Design and development of multiparticulate system for targeted drug delivery to colon. *Drug Deliv. J. Deliv. Target. Ther. Agents* **2004**, *11*, 201–207.
45. Moustafine, R.I.; Margulis, E.B.; Sibgatullina, L.F.; Kemenova, V.A.; Van den Mooter, G. Comparative evaluation of interpolyelectrolyte complexes of chitosan with Eudragit® L100 and Eudragit® L100-55 as potential carriers for oral controlled drug delivery. *Eur. J. Pharm. Biopharm.* **2008**, *70*, 215–225.
46. Xu, B.; Zhang, W.; Chen, Y.; Xu, Y.; Wang, B.; Zong, L. Eudragit® L100-coated mannosylated chitosan nanoparticles for oral protein vaccine delivery. *Int. J. Biol. Macromol.* **2018**, *113*, 534–542.

47. Ghaffari, A.; Navaee, K.; Oskoui, M.; Bayati, K.; Rafiee-Tehrani, M. Preparation and characterization of free mixed-film of pectin/chitosan/Eudragit® RS intended for sigmoidal drug delivery. *Eur. J. Pharm. Biopharm.* **2007**, *67*, 175–186.
48. Kouchak, M.; Handali, S.; Naseri Boroujeni, B. Evaluation of the mechanical properties and drug permeability of chitosan/Eudragit RL composite film. *Osong Public Health Res. Perspect.* **2015**, *6*, 14–19.
49. Bartmański, M.; Pawłowski, Ł.; Zieliński, A.; Mielewczyk-Gryń, A.; Strugała, G.; Cieślik, B. Electrophoretic deposition and characteristics of chitosan/nanosilver composite coatings on the nanotubular TiO_2 layer. *Coatings* **2020**, *10*, 245.
50. International Standard ISO 4287-1997. Geometrical Product Specifications (GPS) – Surface Texture: Profile Method – Terms, Definitions and Surface Texture Parameters, Geneva, Switzerland, **1997**.
51. Loch, J.; Krawiec, H. Corrosion behaviour of cobalt alloys in artificial saliva solution. *Arch. Foundry Eng.* **2013**, *13*, 101–106.
52. Yang, J.; Dahlström, C.; Edlund, H.; Lindman, B.; Norgren, M. pH-responsive cellulose–chitosan nanocomposite films with slow release of chitosan. *Cellulose* **2019**, *26*, 3763–3776.
53. Lim, H.S.; Hwang, M.J.; Jeong, H.N.; Lee, W.Y.; Song, H.J.; Park, Y.J. Evaluation of surface mechanical properties and grindability of binary Ti alloys containing 5 wt % Al, Cr, Sn, and V. *Metals (Basel)* **2017**, *7*, 487.
54. Sorkhi, L.; Farrokhi-Rad, M.; Shahrabi, T. Electrophoretic deposition of hydroxyapatite–chitosan–titania on stainless steel 316 L. *Surfaces* **2019**, *2*, 458–467.
55. Gebhardt, F.; Seuss, S.; Turhan, M.C.; Hornberger, H.; Virtanen, S.; Boccaccini, A.R. Characterization of electrophoretic chitosan coatings on stainless steel. *Mater. Lett.* **2012**, *66*, 302–304.
56. Sorkhi, L.; Farrokhi-Rad, M.; Shahrabi, T. Electrophoretic deposition of chitosan in different alcohols. *J. Coat. Technol. Res.* **2014**, *11*, 739–746.
57. Kowalski, P.; Łosiewicz, B.; Goryczka, T. Deposition of chitosan layers on NiTi shape memory alloy. *Arch. Metall. Mater.* **2015**, *60*, 171–176.
58. Pawlik, A.; Rehman, M.A.U.; Nawaz, Q.; Bastan, F.E.; Sulka, G.D.; Boccaccini, A.R. Fabrication and characterization of electrophoretically deposited chitosan-hydroxyapatite composite coatings on anodic titanium dioxide layers. *Electrochim. Acta* **2019**, *307*, 465–473.
59. Grandfield, K.; Zhitomirsky, I. Electrophoretic deposition of composite hydroxyapatite-silica-chitosan coatings. *Mater. Charact.* **2008**, *59*, 61–67.
60. Jugowiec, D.; Kot, M.; Moskalewicz, T. Electrophoretic deposition and characterisation of chitosan coatings on near-β titanium alloy. *Arch. Metall. Mater.* **2016**, *61*, 657–664.
61. Feng, B.; Weng, J.; Yang, B.C.; Qu, S.X.; Zhang, X.D. Characterization of surface oxide films on titanium and adhesion of osteoblast. *Biomaterials* **2003**, *24*, 4663–4670.
62. Linares, V.; Yarce, C.J.; Echeverri, J.D.; Galeano, E.; Salamanca, C.H. Relationship between degree of polymeric ionisation and hydrolytic degradation of Eudragit® E polymers under extreme acid conditions. *Polymers (Basel)* **2019**, *11*, 1010.
63. Abdeen, Z.; Mohammad, S.G.; Mahmoud, M.S. Adsorption of Mn (II) ion on polyvinyl alcohol/chitosan dry blending from aqueous solution. *Environ. Nanotechnol. Monit. Manag.* **2015**, *3*, 1–9.
64. Dimzon, I.K.D.; Knepper, T.P. Degree of deacetylation of chitosan by infrared spectroscopy and partial least squares. *Int. J. Biol. Macromol.* **2015**, *72*, 939–945.
65. Kumar, B.P.; Archana, G. Formulation and evaluation of nizatidine solid dispersions. *World J. Pharm. Pharm. Sci.* **2015**, *4*, 810–817.
66. Niinomi, M.; Nakai, M.; Hieda, J. Development of new metallic alloys for biomedical applications. *Acta Biomater.* **2012**, *8*, 3888–3903.
67. Bartmański, M.; Pawłowski, Ł.; Strugała, G.; Mielewczyk-Gryń, A.; Zieliński, A. Properties of nanohydroxyapatite coatings doped with nanocopper, obtained by electrophoretic deposition on Ti13Zr13Nb alloy. *Materials (Basel)* **2019**, *12*, 3741.
68. Hryniewicz, T.; Rokosz, K.; Rokicki, R.; Prima, F. Nanoindentation and XPS studies of titanium TNZ alloy after electrochemical polishing in a magnetic field. *Materials (Basel)* **2015**, *8*, 205–215.
69. Drevet, R.; Jaber, N.B.; Fauré, J.; Tara, A.; Larbi, A.B.C.; Benhayoune, H. Electrophoretic deposition (EPD) of nano-hydroxyapatite coatings with improved mechanical properties on prosthetic Ti6Al4V substrates. *Surf. Coatings Technol.* **2016**, *301*, 94–99.

70. Sidane, D.; Chicot, D.; Yala, S.; Ziani, S.; Khireddine, H.; Iost, A.; Decoopman, X. Study of the mechanical behavior and corrosion resistance of hydroxyapatite sol-gel thin coatings on 316 L stainless steel pre-coated with titania film. *Thin Solid Films* **2015**, *593*, 71–80.
71. Wang, Y.C.; Leu, I.C.; Hon, M.H. Kinetics of electrophoretic deposition for nanocrystalline zinc oxide coatings. *J. Am. Ceram. Soc.* **2004**, *87*, 84–88.
72. Díez-Pascual, A.M.; Gómez-Fatou, M.A.; Ania, F.; Flores, A. Nanoindentation in polymer nanocomposites. *Prog. Mater. Sci.* **2015**, *67*, 1–94.
73. Fahim, I.S.; Aboulkhair, N.; Everitt, N.M. Nanoindentation investigation on chitosan thin films with different types of nano fillers. *J. Mater. Sci. Res.* **2018**, *7*, 11.
74. Akhtar, M.A.; Hadzhieva, Z.; Dlouhy, I.; Boccaccini, A.R. Electrophoretic deposition and characterization of functional coatings based on an antibacterial gallium (III)-chitosan complex. *Coatings* **2020**, *10*, 483.
75. Stevanović, M.; Došić, M.; Janković, A.; Kojić, V.; Vukašinović-Sekulić, M.; Stojanović, J.; Odović, J.; Crevar Sakač, M.; Rhee, K.Y.; Mišković-Stanković, V. Gentamicin-loaded bioactive hydroxyapatite/chitosan composite coating electrodeposited on titanium. *ACS Biomater. Sci. Eng.* **2018**, *4*, 3994–4007.
76. Brohede, U.; Zhao, S.; Lindberg, F.; Mihranyan, A.; Forsgren, J.; Strømme, M.; Engqvist, H. A novel graded bioactive high adhesion implant coating. *Appl. Surf. Sci.* **2009**, *255*, 7723–7728.
77. Zhang, J.; Dai, C.S.; Wei, J.; Wen, Z.H. Study on the bonding strength between calcium phosphate/chitosan composite coatings and a Mg alloy substrate. *Appl. Surf. Sci.* **2012**, *261*, 276–286.
78. Szymańska, E.; Winnicka, K. Stability of chitosan—A challenge for pharmaceutical and biomedical applications. *Mar. Drugs* **2015**, *13*, 1819–1846.
79. Pawłowski, Ł.; Bartmański M.; Zieliński A. pH-dependent composite coatings for controlled drug delivery system—Review. *Inżynieria Mater.* **2019**, *1*, 4–9.
80. Boeris, V.; Romanini, D.; Farruggia, B.; Picó, G. Interaction and complex formation between catalase and cationic polyelectrolytes: Chitosan and Eudragit E100. *Int. J. Biol. Macromol.* **2009**, *45*, 103–108.
81. Bagherifard, S. Mediating bone regeneration by means of drug eluting implants: From passive to smart strategies. *Mater. Sci. Eng. C* **2017**, *71*, 1241–1252.
82. Zheng, K.; Setyawati, M.I.; Leong, D.T.; Xie, J. Antimicrobial silver nanomaterials. *Coord. Chem. Rev.* **2018**, *357*, 1–17.
83. Thinakaran, S.; Loordhuswamy, A.; Rengaswami, G.V. Electrophoretic deposition of chitosan/nano silver embedded micro sphere on centrifugal spun fibrous matrices—A facile biofilm resistant biocompatible material. *Int. J. Biol. Macromol.* **2020**, *148*, 68–78.
84. Fayomi, O.S.I.; Akande, I.G.; Popoola, A.P.I. Corrosion protection effect of chitosan on the performance characteristics of A6063 alloy. *J. Bio- Tribo-Corros.* **2018**, *4*, 1–6.
85. Mareci, D.; Ungureanu, G.; Aelenei, D.M.; Mirza Rosca, J.C. Electrochemical characteristics of titanium based biomaterials in artificial saliva. *Mater. Corros.* **2007**, *58*, 848–856.
86. Qu, Q.; Wang, L.; Chen, Y.; Li, L.; He, Y.; Ding, Z. Corrosion behavior of titanium in artificial saliva by lactic acid. *Materials (Basel)* **2014**, *7*, 5528–5542.
87. Chen, Q.; Thouas, G.A. Metallic implant biomaterials. *Mater. Sci. Eng. R Rep.* **2015**, *87*, 1–57.
88. Surmeneva, M.A.; Sharonova, A.A.; Chernousova, S.; Prymak, O.; Loza, K.; Tkachev, M.S.; Shulepov, I.A.; Epple, M.; Surmenev, R.A. Incorporation of silver nanoparticles into magnetron-sputtered calcium phosphate layers on titanium as an antibacterial coating. *Colloids Surf. B Biointerfaces* **2017**, *156*, 104–113.
89. Demczuk, A.; Swieczko-Zurek, B.; Ossowska, A. Corrosion resistance examinations of Ti6Al4V alloy with the use of potentiodynamic method in ringer's and artificial saliva solutions. *Adv. Mater. Sci.* **2012**, *11*, 4–11.
90. Bartmanski, M.; Zielinski, A.; Jazdzewska, M.; Głodowska, J.; Kalka, P. Effects of electrophoretic deposition times and nanotubular oxide surfaces on properties of the nanohydroxyapatite/nanocopper coating on the Ti13Zr13Nb alloy. *Ceram. Int.* **2019**, *45*, 20002–20010.
91. Heise, S.; Forster, C.; Heer, S.; Qi, H.; Zhou, J.; Virtanen, S.; Lu, T.; Boccaccini, A.R. Electrophoretic deposition of gelatine nanoparticle/chitosan coatings. *Electrochim. Acta* **2019**, *307*, 318–325.
92. Cordero-Arias, L.; Cabanas-Polo, S.; Gao, H.; Gilabert, J.; Sanchez, E.; Roether, J.A.; Schubert, D.W.; Virtanen, S.; Boccaccini, A.R. Electrophoretic deposition of nanostructured-TiO_2/chitosan composite coatings on stainless steel. *RSC Adv.* **2013**, *3*, 11247–11254.